



Endothelial vacuolization induced by highly permeable silicon membranes



Barrett J. Nehilla^{a,1}, Nakul Nataraj^{b,2}, Thomas R. Gaboriski^{b,3}, James L. McGrath^{a,*}

^aDepartment of Biomedical Engineering, Box 270168, University of Rochester, Rochester, NY 14627, USA

^bSIMPore Inc., 150 Lucius Gordon Dr. Suite 119, West Henrietta, NY 14586, USA

ARTICLE INFO

Article history:

Received 15 March 2014

Received in revised form 14 June 2014

Accepted 18 July 2014

Available online 27 July 2014

Keywords:

Nanoporous materials

Biomaterials

Silicon

Membranes

Tissue engineering

ABSTRACT

Assays for initiating, controlling and studying endothelial cell behavior and blood vessel formation have applications in developmental biology, cancer and tissue engineering. In vitro vasculogenesis models typically combine complex three-dimensional gels of extracellular matrix proteins with other stimuli like growth factor supplements. Biomaterials with unique micro- and nanoscale features may provide simpler substrates to study endothelial cell morphogenesis. In this work, patterns of nanoporous, nanothin silicon membranes (porous nanocrystalline silicon, or pnc-Si) are fabricated to control the permeability of an endothelial cell culture substrate. Permeability on the basal surface of primary and immortalized endothelial cells causes vacuole formation and endothelial organization into capillary-like structures. This phenomenon is repeatable, robust and controlled entirely by patterns of free-standing, highly permeable pnc-Si membranes. Pnc-Si is a new biomaterial with precisely defined micro- and nanoscale features that can be used as a unique in vitro platform to study endothelial cell behavior and vasculogenesis.

© 2014 Acta Materialia Inc. Published by Elsevier Ltd. All rights reserved.

1. Introduction

Biomaterials with nanoscale dimensions and structures can be used to control cell adhesion, morphology and function in vitro and in vivo. Silicon is often used for nanomaterials because of its simple, highly controllable, scalable and inexpensive manufacturing. Work with porous silicon substrates has demonstrated that nanostructured silicon is biocompatible for cell culture in vitro [1] and as a cell support in vivo [2]. Since then, nanostructured silicon biomaterials have been used in many biomedical applications: membranes for immunoisolation of medical implants, particulates for pharmaceutical delivery, imaging probes, and surface cues to alter cell adhesion, morphology and inflammatory responses [3–5]. Porous nanocrystalline silicon (pnc-Si) is a new type of porous silicon characterized by nanoscale through-pores and nanometer thickness in defined, microscale free-standing membrane areas. Tight control over pnc-Si pore diameters (~5–100 nm) allows

size-dependent separation of biomolecules and other nanoparticles with size selectivity as low as 5.0 nm [6,7]. Experimental observations of biomolecule diffusion through porous membranes showed good agreement with theoretical predictions [8]. The negligible thickness (~5–60 nm) of pnc-Si membranes affords remarkably high hydraulic and gas permeability [7,9]. These fundamental properties make pnc-Si a unique nanomaterial for chemical, biomolecule and nanoparticle separations.

Studies have established that pnc-Si, like porous silicon, is biocompatible. Specifically, primary and immortalized mammalian cells adhere to pnc-Si with an efficiency nearly identical to that of common cell culture substrates such as glass and polystyrene [10]. The cells exhibited typical morphologies, proliferated normally and remained viable after several days of culture [10]. Pnc-Si chips are incorporated easily into plastic housings that mimic commercial transwell cell culture devices. However, unlike commercial transwells with 10 μm thick membranes, pnc-Si transwells boast a nanometers-thick, highly permeable and optically transparent pnc-Si membrane. The biocompatibility of pnc-Si membranes and their molecular-scale thinness affords a unique opportunity to create in vitro mimics of biological tissue. For example, in the blood–brain barrier (BBB), astrocytic end feet are separated from the abluminal surface of brain endothelial cells by ~20 nm [11]. Many in vitro BBB models establish co-cultures of endothelial cells and astrocytes on opposite sides of commercial transwell

* Corresponding author. Tel.: +1 585 273 5489; fax: +1 585 273 4746.

E-mail address: jmcgrath@bme.rochester.edu (J.L. McGrath).

¹ Present address: Nexgenia, Inc., Fluke Hall, 4000 Mason Rd., Seattle, WA 98195, USA.

² Present address: Acrometrix, A Division of Life Technologies, ThermoFisher, Benicia, CA 04510, USA.

³ Present address: Rochester Institute of Technology, Biomedical Engineering Program, Rochester, NY 14623, USA.

membranes [12,13] that are 1000× thicker than the in vivo spacing. During development of a BBB co-culture model on pnc-Si transwells with anatomically accurate separation (~30 nm) between endothelium and astrocytes [11], interesting endothelial cell behavior was discovered on nanoporous, nanothin pnc-Si membranes.

In this work, endothelial cells were grown on 30 nm thick, free-standing, nanoporous pnc-Si membranes patterned adjacent to impermeable pnc-Si in custom transwell culture devices. Surprisingly, endothelial cells were found to express vacuoles and organize into capillary-like structures in a manner that required substrate permeability. Previously, such hallmarks of vasculogenesis were only seen when cells were grown in 3-D constructs of extracellular matrix (ECM) proteins or hydrogels and with the addition of pro-angiogenic growth factors [14–19]. The apparent ability of pnc-Si membranes to trigger elements of the vasculogenesis program in endothelial cells without the addition of pro-angiogenic conditions suggests that substrate permeability itself can influence cell maturation and morphogenesis. The possibility of controlling endothelial cell behavior with 2-D patterns of free-standing pnc-Si membranes makes pnc-Si a new tool for in vitro angiogenesis assays and for promoting vessel formation in tissue engineering applications.

2. Materials and methods

2.1. Pnc-Si fabrication and transwell assembly

Pnc-Si membranes were fabricated using standard semiconductor processes, as described elsewhere [6] and in the online [supplementary material](#). Each silicon wafer was designed to yield ~80 samples, or chips. Each chip contained two ~2000 μm × 100 μm slits with free-standing 30 nm thick pnc-Si membranes containing pores with diameters ~15 nm. The pnc-Si chips were secured in custom-designed polypropylene housings (Harbec Plastics, Inc., Ontario, NY) to mimic the geometry of commercial transwell devices (Fig. 1). Pnc-Si transwells were autoclaved before use.

2.2. Fabrication of microporous silicon nitride membranes

Microporous, nano-thin silicon nitride (SiN) membranes were fabricated using semiconductor processing techniques similar to previous reports [20,21] and further described in the [supplementary material](#). The pores were patterned as 3 μm circles on a rectangular coordinate system with a 6 μm center-center spacing, resulting in 22.7% porosity. The silicon nitride membrane was 50 nm thick. Chips were manually cleaved from the wafer and inspected optically, by scanning and transmission electron microscopy (SEM/TEM).

2.3. Cell culture

Cell studies were performed with bEnd.3 mouse brain endothelial cells [22] from ATCC (Rockville, MD, USA), primary human umbilical vein endothelial cells (HUVECs; Microbiology & Immunology Lab, University of Rochester Medical Center, Rochester, NY, USA) and mouse embryo fibroblasts (3T3-L1, ATCC). Routine cell culture was performed as described in the [supplementary material](#). After trypsinization, cells were seeded on the bottom surface of transwells at 5×10^5 cells cm⁻², allowed to attach and then grown upside-down for all experiments (Fig. 1C). Cell culture on pnc-Si transwells was compared to commercial PET Transwells® with 0.4 μm pore diameters (Corning), or on tissue culture-treated polystyrene (TCPS). On silicon nitride membranes with 3 μm pore

diameters, cells were seeded (2.5×10^6 cells ml⁻¹) and grown for 3 days on SimPore CytoVu® imaging slides before analysis.

2.4. Live/dead staining

After specified growth periods, calcein-AM (2 μM) and ethidium bromide (4 μM) were incubated with cells for 30 min in the dark at 21 °C. Cells were gently rinsed with Hanks' balanced salt solution (HBSS) and observed with an inverted epifluorescent Nikon Eclipse TS-100F microscope equipped with a Cooke Sensicam HP cooled CCD camera (20× objective). Phase contrast, green and red fluorescent images were acquired for each sample. Green and red channels were overlaid in ImageJ 1.4G, and free-standing pnc-Si areas were delineated in Adobe Illustrator CS3. If needed, brightness and contrast adjustment were applied to entire image files in ImageJ before cropping in Adobe Photoshop CS3 for presentation. Vacuoles were counted on three different samples of free-standing pnc-Si, supported pnc-Si, PET and TCPS, and data were presented as the mean with standard deviations as error bars (Fig. 2D).

2.5. Vacuole experiments

To study nucleus–vacuole co-localization, bEnd.3 cells were grown for 1 day on pnc-Si transwells and then stained with calcein-AM (2 μM) and Hoechst 33342 (1 μM). After rinsing with HBSS, samples were observed with an inverted epifluorescent Zeiss Axiovert 200 M microscope equipped with a Cooke Sensicam cooled CCD camera (20× objective). Phase-contrast, blue and green fluorescent images were acquired for each sample.

To investigate fluid uptake into vacuoles, growth media with 6-carboxyfluorescein (60 μg ml⁻¹) was added to bEnd.3 cells immediately after seeding. Cells were cultured for 1 day in this media and then rinsed extensively in HBSS to remove unincorporated dye. Phase-contrast and green fluorescent images were acquired for each sample with the Nikon system.

The bEnd.3 cells were cultured on PET and pnc-Si transwells for 1 day in order to allow vacuole formation. To inhibit vacuole formation, normal growth media was replaced with media containing bafilomycin A1 (10 nM). After 1 day of culture in bafilomycin A1, cells were stained with live/dead solution and observed with the Nikon system.

To test whether permeability or membrane mechanics controlled vacuole formation, the flat side of pnc-Si samples was adhered to cloning rings with vacuum grease. Then, cells were adhered to pnc-Si samples in media (~300 μl), and these cloning ring samples were inverted into Petri dishes. To block the pnc-Si permeability but maintain fluid on both sides of the cells, a drop of media was applied to the well side and then limited to the well volume (~300 nl) with a coverslip. Control samples were prepared by attaching another cloning ring to the well-side of pnc-Si and filling it with media (~300 μl).

2.6. Diffusion measurements

Hydrogen peroxide (H₂O₂) and sodium fluorescein (NaF) diffusion were studied with pnc-Si transwells. H₂O₂ (200 μl, 300 μM, $n = 3$) or NaF (200 μl, 19.94 μM, $n = 2$) was added to the apical well of transwells and allowed to diffuse across pnc-Si membranes into the basolateral volume (1 ml) for 24 h. H₂O₂ concentrations in the basolateral well (the “diffusate”) were quantified with the Amplex Red assay kit (Invitrogen). NaF concentrations were quantified by measuring the fluorescence intensity (excitation/emission wavelengths = 485 nm/520 nm) of the basolateral well in a Tecan Infinite 200 M fluorescence microplate reader. To study cytochrome C diffusion, 400 μl of 2 mg ml⁻¹ cytochrome C in PBS was added to the apical well of pnc-Si transwells ($n = 2$), and PBS (40 μl)

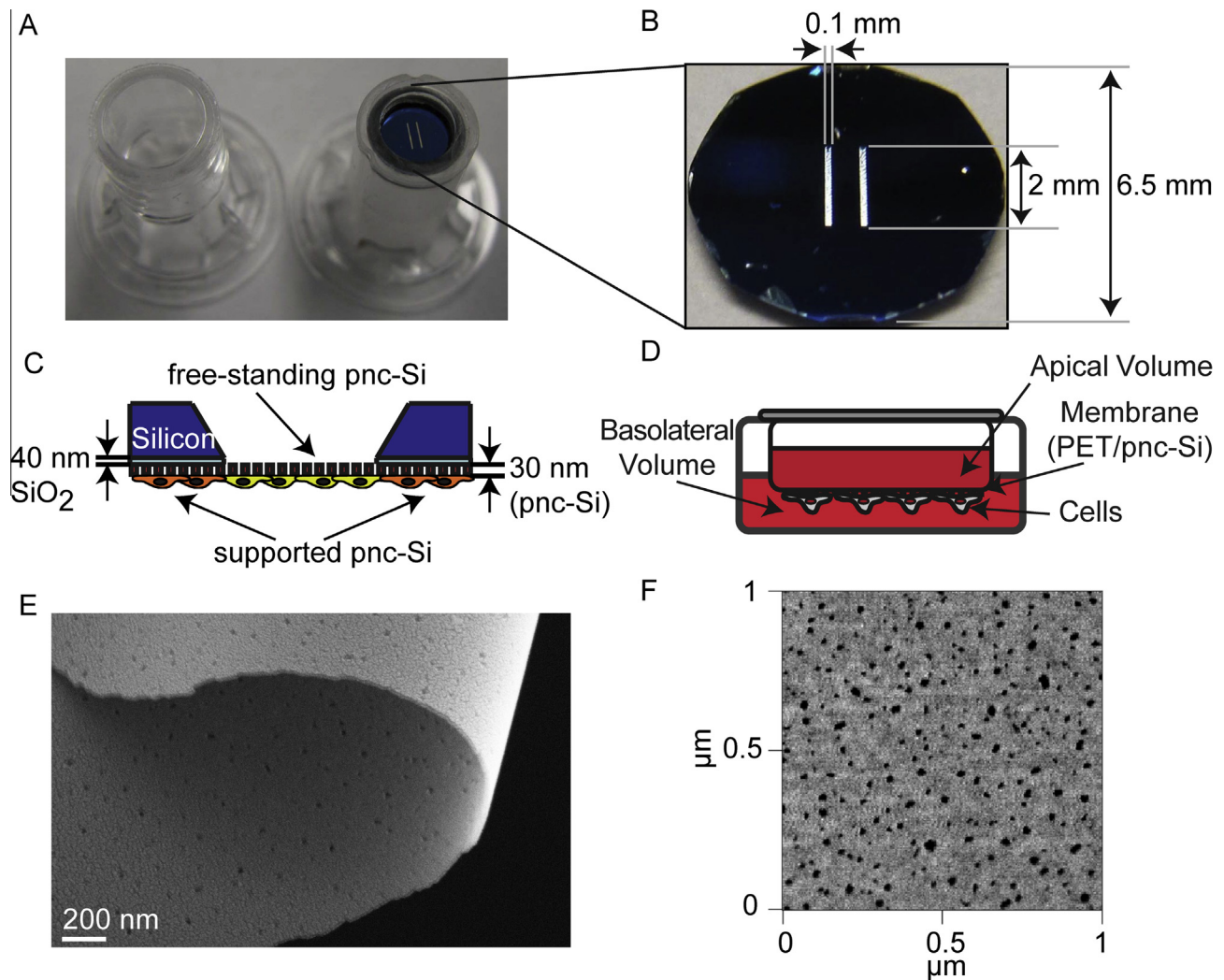


Fig. 1. The transwell configuration and nanoscale structure of pnc-Si. (A) Bottom view of commercial PET (left) and pnc-Si (right) transwells for cell culture in 24-well plates. (B) Geometry of an individual pnc-Si chip, which shows two slits of $\sim 2 \text{ mm} \times 0.1 \text{ mm}$ free-standing pnc-Si surrounded by supported pnc-Si. (C) Side view geometry of pnc-Si chip for cell culture. (D) Side view schematic of a transwell device with apical and basolateral volumes separated by membrane material and cultured cells. The relative height of the apical and basolateral media volumes is not representative of all experiments with pnc-Si transwells. (E) SEM micrograph of broken and folded, free-standing pnc-Si illustrates the $\sim 30 \text{ nm}$ membrane thinness and nanoporous topography. (F) AFM scan of pnc-Si membrane illustrates the relatively monodisperse distribution of pnc-Si nanopore sizes.

was added to the basolateral side of the transwell. After 24 h at 4°C , the protein concentration of the apical and basolateral volumes was quantified by absorbance values at 410 nm . Control transwells contained pnc-Si chips without membranes.

2.7. Statistical analyses

Calculated data were presented as mean values \pm standard deviations. In Fig. 2, a one-way ANOVA and Tukey post hoc analysis determined differences with significance at $P=0.01$. In Fig. 4, differences between typical and low-porosity samples were calculated by an unpaired t -test with significance at $P=0.01$.

3. Results

3.1. Pnc-Si and pnc-Si transwells

Pnc-Si chips were assembled into custom transwell housings that mimicked commercial devices like Corning Transwell[®] inserts (Fig. 1A). Two rectangular slits designed to be $2000 \mu\text{m} \times 100 \mu\text{m}$

(actual area = $182,877.3 \pm 67,047.2 \mu\text{m}^2$, $n=3$ chips) defined the highly permeable, nanoporous, nanocrystalline, free-standing pnc-Si membrane (Fig. 1B). The remaining area, “supported pnc-Si” (Fig. 1C), is also nanoporous and nanocrystalline but impermeable because it is supported on underlying layers of silicon and SiO_2 . Pnc-Si transwells were assembled by securing pnc-Si samples in custom biocompatible polypropylene housings such that free-standing pnc-Si separated apical and basolateral media volumes (Fig. 1A, C, D). The 30 nm ultrathin pnc-Si membrane (Fig. 1E) is robust; pnc-Si transwells can be autoclaved and handled without tearing. Before using samples for cell culture, pore size distributions of pnc-Si samples were quantified from either TEM micrographs or atomic force microscopy (AFM) scans (Fig. 1F). Typical pore diameters were $14.7 \pm 2.1 \text{ nm}$ with membrane porosity of $5.6 \pm 2.1\%$ ($n=3$ chips, 100s of pores), and samples always exhibited a sharp cut-off near the largest pore size.

3.2. Endothelial cells form vacuoles on free-standing pnc-Si

Interesting endothelial cell behavior was discovered when the mouse brain endothelial cell line, bEnd.3, was cultured on the

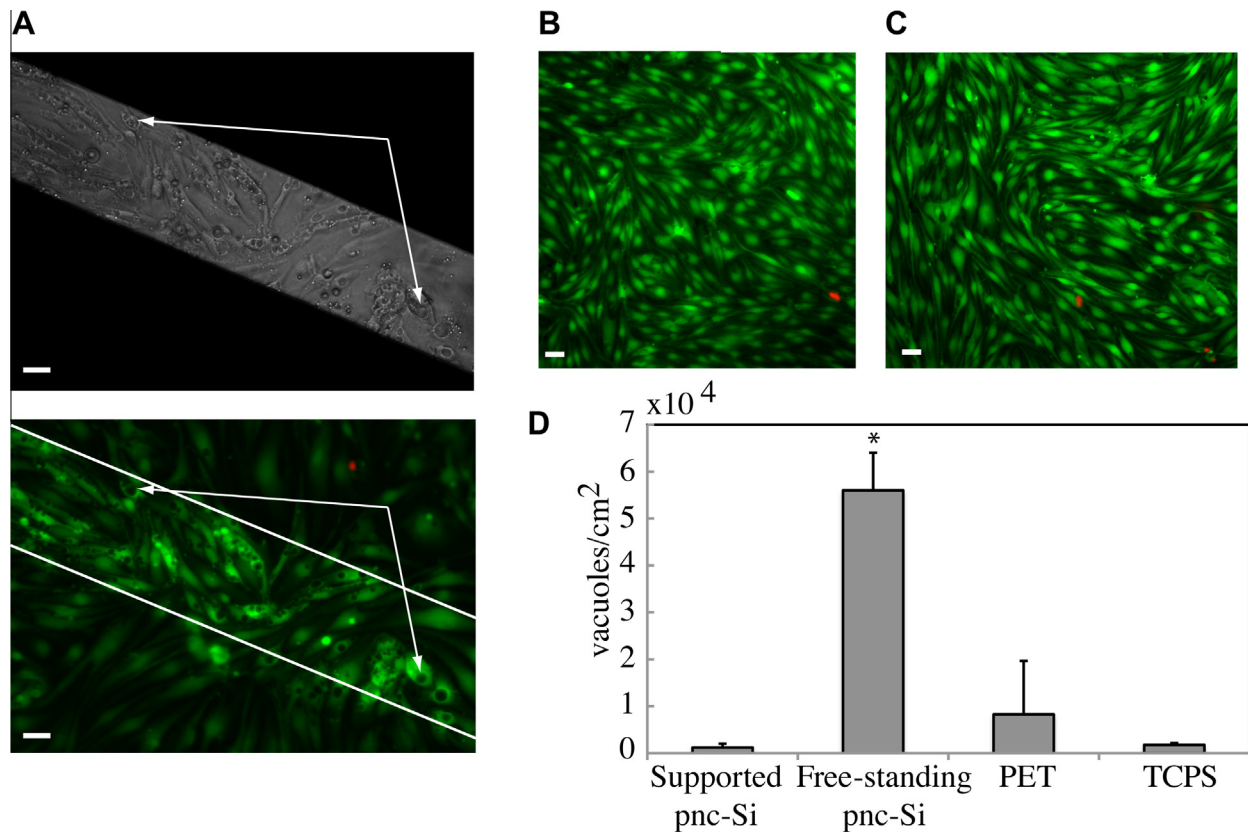


Fig. 2. Vacuole formation in endothelial cells is determined by patterns of highly permeable, free-standing pnc-Si membranes. (A) Phase-contrast (top panel) and fluorescence (bottom panel) images of bEnd.3 cells grown on pnc-Si transwells show non-fluorescent, well-defined regions, presumably vacuoles, within cells only on free-standing membranes (delineated by white lines). Arrows specify vacuoles in two different cells. (B) On PET membranes, very few bEnd.3 cells expressed vacuoles within the cytoplasm. (C) Cells cultured on impermeable tissue culture plastic had no vacuoles. (D) The number of ‘holes’, or vacuoles, expressed in cells per unit area of different culture surfaces. There are more ‘holes’ on free-standing pnc-Si than the other surfaces ($F = 42.52$, $^*P < 0.01$). Red fluorescence in (A–C) was from dead cells. Scale bars = 30 μm .

underside of pnc-Si transwells. In phase-contrast images (Fig. 2A, top), the free-standing pnc-Si membrane was transparent, which revealed well-defined regions of unstained ‘holes’ within cells. Cells on free-standing and supported pnc-Si areas were visible in fluorescent images (Fig. 2A, bottom), which showed that the unstained ‘holes’ (arrows) were limited to the free-standing pnc-Si area (between the white lines). These unstained regions were observed within 1 day of cell adhesion and persisted for more than 2 weeks. In contrast, for cultures on commercial polyester (PET) transwells with 0.4 μm pore diameters, 10 μm thickness and $\sim 100\times$ less permeability, very few unstained regions were identified across the entire membrane area (Fig. 2B). Even fewer unstained regions were found after growing cells for 2 weeks on impermeable TCPS (Fig. 2C). For all surfaces, very few dead (red fluorescent) cells were observed. The number of these unstained regions on supported pnc-Si (1196.0 ± 810.7), free-standing pnc-Si (56020.1 ± 8045.4), PET (8257.5 ± 11410.0) and TCPS (1747.6 ± 363.8) was quantified (Fig. 2D, $n = 3$), which showed that cell ‘holes’ were highly localized on free-standing pnc-Si. Based on their frequency and distribution within the cytoplasm of bEnd.3 cells, we hypothesized that these ‘holes’ were vacuoles.

Several experiments confirmed that unstained ‘holes’ in bEnd.3 cells were vacuoles. The ‘holes’ in the green fluorescent cytoplasm (calcein AM) did not overlap with blue fluorescent (Hoechst 33342) nuclei (Fig. 3A). On the other hand, the cell ‘holes’ were loaded with the cell membrane-impermeant dye 6-carboxyfluorescein (6-CF, Fig. 3B). The cell ‘holes’ were well resolved in phase-contrast images (left panel). Co-localization of a ‘hole’ in phase contrast with green fluorescence from 6-CF (right

panel) suggested that 6-CF was pinocytosed by cells from the culture media and concentrated within fluid-filled vacuolar membranes. Other groups have used fluorescent dyes to label vacuoles as well [14,23,24]. Low doses of the vacuolar-type H(+)-ATPase inhibitor bafilomycin A1 (10 nM) prevented expression of the unstained regions over free-standing pnc-Si (Fig. 3C) without altering cell morphology. Although some dead (red fluorescent) cells were seen, overall cell viability remained high. Bafilomycin A1 also inhibited drug-induced vacuole formation in endothelial cells [25] and other cell types [26]. These complementary studies showed that the ‘holes’ in bEnd.3 cells over free-standing pnc-Si membranes were vacuoles.

Primary HUVECs also displayed vacuoles after a day of culture on pnc-Si (Supplementary Fig. 1A), while immortalized 3T3-L1 fibroblasts did not (Supplementary Fig. 1B). Thus, while the induction of vacuoles on pnc-Si was not a universal response, it was characteristic of at least two types of vascular endothelial cells. Interestingly, the fibroblasts also appeared to respond to pnc-Si. These cells grew more densely and with 3-D structure only over the free-standing membrane regions of the pnc-Si transwells (Supplementary Fig. 1B).

3.3. Vacuole formation is a response to substrate permeability

We hypothesized that substrate permeability was the environmental variable responsible for vacuole formation due to trends in vacuole formation: bEnd.3 cells displayed many vacuoles on highly permeable, free-standing pnc-Si, fewer vacuoles on low-permeability polymer membranes and no vacuoles on

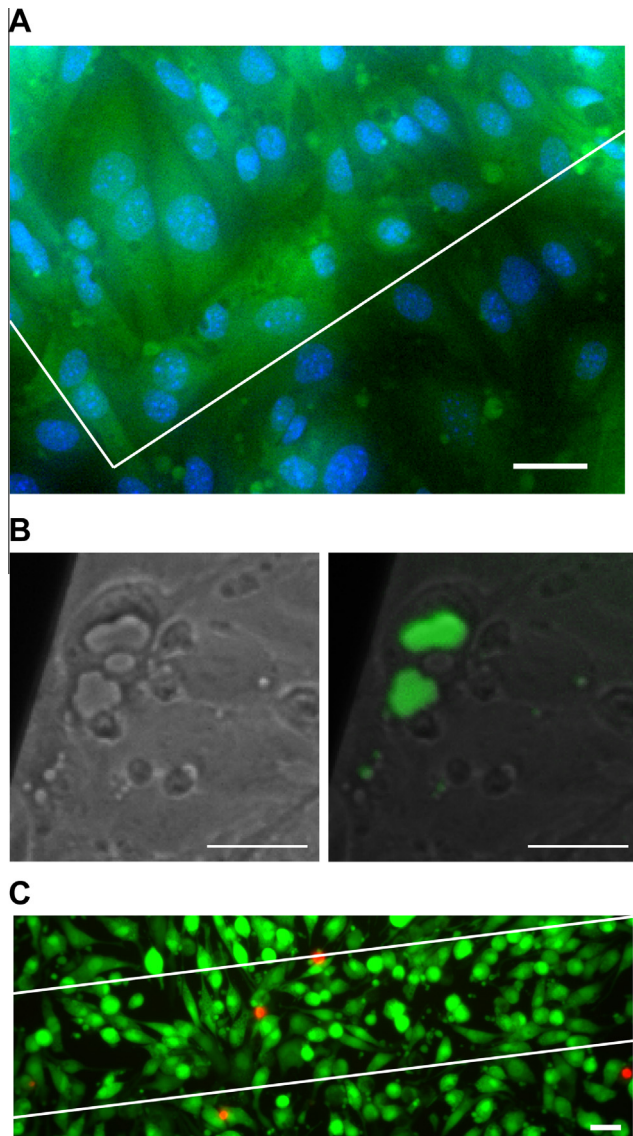


Fig. 3. Unlabeled regions within live/dead-stained cells are vacuoles. (A) bEnd.3 cells stained simultaneously with green calcein-AM (live cell cytoplasm) and blue Hoechst 33342 (nucleus) showed no overlap between unstained vacuoles and blue nuclei. (B) Vacuoles in a phase-contrast image (left panel) were loaded with green fluorescent 6-carboxyfluorescein, a fluid-phase marker, in an overlay image (right panel). (C) Treatment of bEnd.3 cells with 10 nM bafilomycin A1, a vacuolar-type (H⁺)-ATPase inhibitor, abrogated vacuole expression within 24 h. Scale bars = 30 μ m.

impermeable pnc-Si or TCPS. The first test of this hypothesis compared vacuole formation on normal (Fig. 4A, top) and low-porosity (Fig. 4A, bottom) pnc-Si samples. The low-porosity samples were produced with lower annealing temperatures during pore formation [6,27]. TEM scans of low-porosity membranes showed no through-pores, indicating that any pores in these membranes were smaller than the TEM resolution (≤ 2 nm). Therefore, the pore size was measured indirectly by examining the diffusion of a molecular size ladder consisting of H₂O₂ (34 Da), NaF (383 Da) and cytochrome C (13 kDa). The hydrodynamic radius of these molecules was 0.16 nm [28], 0.46 nm [29] and 2.1 nm [30], respectively, which was calculated via the Stokes–Einstein relationship and published diffusion coefficients. Molecular diffusion measurements (Fig. 4B) across low-porosity pnc-Si samples showed that H₂O₂ freely passed, NaF was slightly hindered, and cytochrome C did not pass. This result suggests that low-porosity membranes have

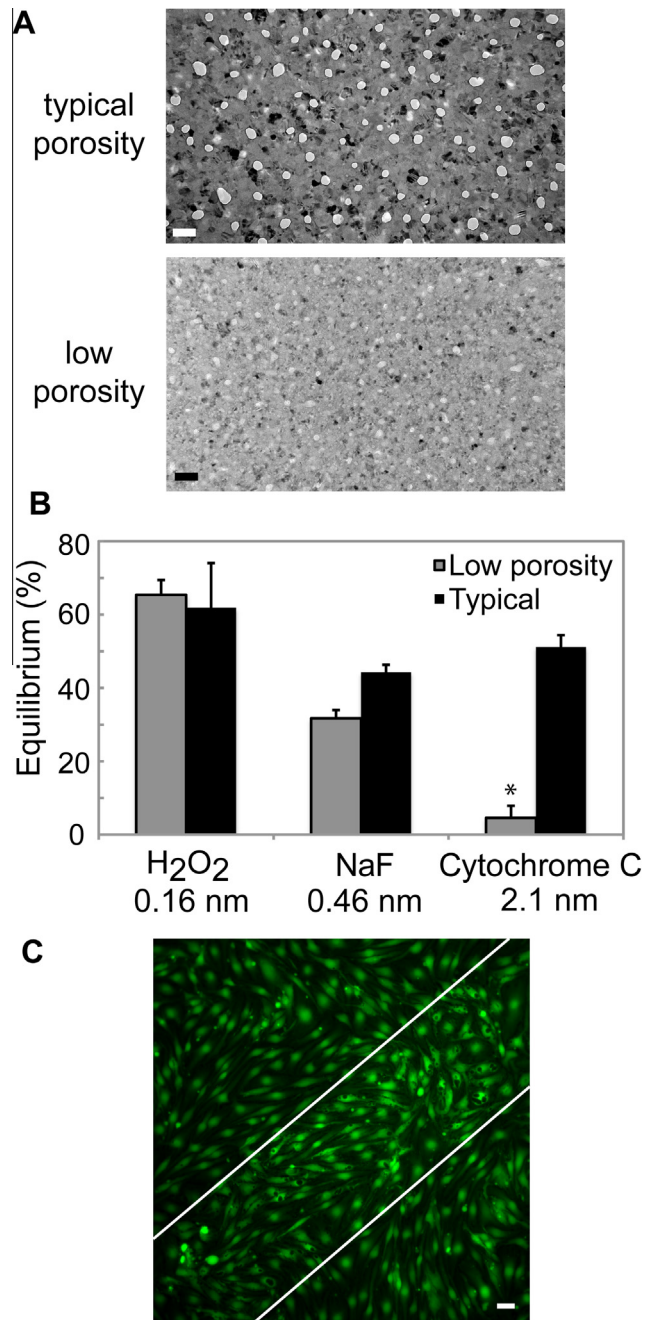


Fig. 4. Low porosity pnc-Si transwells induced endothelial vacuolization. (A) Representative TEM micrographs of a typical pnc-Si sample with 15 nm average pore diameter (top panel) and a low porosity pnc-Si sample with undetectable pores (bottom panel). Scale bars = 50 nm. (B) The diffusion of selected small molecules through typical and low-porosity pnc-Si samples, measured as the percentage of the expected equilibrium concentration. Hydrogen peroxide is not hindered in low-porosity pnc-Si ($P > 0.70$). A slightly larger small molecule, sodium fluorescein (NaF), is slightly hindered ($P = 0.03$). By contrast, cytochrome C has a larger hydrodynamic radius and diffused through typical pnc-Si but not through the low-porosity pnc-Si sample ($*P = 0.0049$). (C) On the low-porosity pnc-Si sample with undetectable pores, bEnd.3 cells expressed vacuoles over free-standing pnc-Si. Scale bar = 30 μ m.

pores ~ 0.5 – 1 nm in diameter and are still highly permeable to small molecules. By contrast, all three molecules easily passed through normal pnc-Si. When bEnd.3 cells were grown on low-porosity pnc-Si, they again displayed vacuoles over free-standing membranes, although the vacuoles were less numerous than on standard pnc-Si (Fig. 4C).

To test if vacuole formation was specific to the pnc-Si material, cells were grown on 50 nm thick microporous SiN (Fig. 5A). These membranes were produced with photolithography techniques developed by others [20,21], and they featured $2.90 \pm 0.08 \mu\text{m}$ pores ($n = 3$ chips, 12 pores). Although these microporous SiN membranes have pore diameters $\sim 100\times$ that of pnc-Si, they are actually less permeable to small molecule diffusion than pnc-Si with ~ 15 nm pores. This is because pore density is the important determinant of diffusion permeability of molecularly thin membranes [8,31]. The bEnd.3 cells developed vacuoles on free-standing SiN (but not on supported SiN) with roughly half the frequency seen on pnc-Si (Fig. 5B). This result clearly indicates that vacuole formation on molecularly thin membranes is not specific to nanoporous pnc-Si. Interestingly, although fewer vacuoles were seen on microporous SiN than on nanoporous pnc-Si, the vacuoles were much larger, which may be related to the fact that SiN membrane pores were also much larger.

Substrate deformability is an important determinant of cell phenotype [32]. We therefore considered an alternative hypothesis that vacuole formation was a response to the fact that free-standing pnc-Si is more deformable than supported pnc-Si. To test this idea, a coverslip was attached to the backside of a pnc-Si chip, which reduced the basal fluid volume to ~ 300 nl. Control samples with hundreds of microliters of media on both sides of the pnc-Si membrane expressed vacuoles (Supplementary Fig. 2A), but cells grown on pnc-Si with blocked basal permeability did not express

vacuoles (Supplementary Fig. 2B). Since blocked and control membranes have the same deformability but elicit different vacuole expression behaviors, a difference in membrane compliance is not responsible for vacuole formation.

One additional piece of evidence suggested that substrate permeability was responsible for vacuole formation in bEnd.3 cells. When free-standing pnc-Si areas were limited to squares about the size of a cell (1750 nm^2), vacuoles formed only in the few cells that were either on top of the free-standing membrane or immediately adjacent to it (Supplementary Fig. 2C). The adjacent cells expressing vacuoles may have responded to the nearby substrate permeability or may have recently migrated away from the free-standing patch. Thus, the induction of vacuoles in endothelial cells is a highly localized, single-cell response to substrate permeability.

3.4. Tubule formation after prolonged culture on pnc-Si

After several days of bEnd.3 growth and vacuole expression on pnc-Si transwells, endothelial cells self-assembled into capillary-like structures and branched networks that followed the free-standing membrane geometry (Fig. 6A). These organized cells extended for hundreds of microns. Higher-resolution images of these structures showed that vacuoles in neighboring cells were directly apposed and elongated (Fig. 6B). Such images suggest a process of vacuole coalescence and lumen formation between adjacent endothelial cells reminiscent of lumen formation *in vivo* [23]. The presence of vacuoles, nascent lumens and organized, multicellular structures on pnc-Si transwells also closely resembles the capillary-like structures created by *in vitro* tubulogenesis assays [14,15,17,23,33]. However, endothelial cell morphogenesis on pnc-Si transwells was elicited without the commonly used media supplements of pro-angiogenic factors (i.e. VEGF, phorbol myristate acetate) [15,34,35].

Interestingly, fibroblasts did not form vacuoles or tubules when cultured on highly permeable pnc-Si, but they—like endothelial cells—did respond by forming a 3-D culture structure over the free-standing membrane. Thus basal permeability may induce phenotype changes in multiple cell types, but the specific response depends on the cell type and its function in native tissue. In the case of endothelial cells, high basal permeability appears to

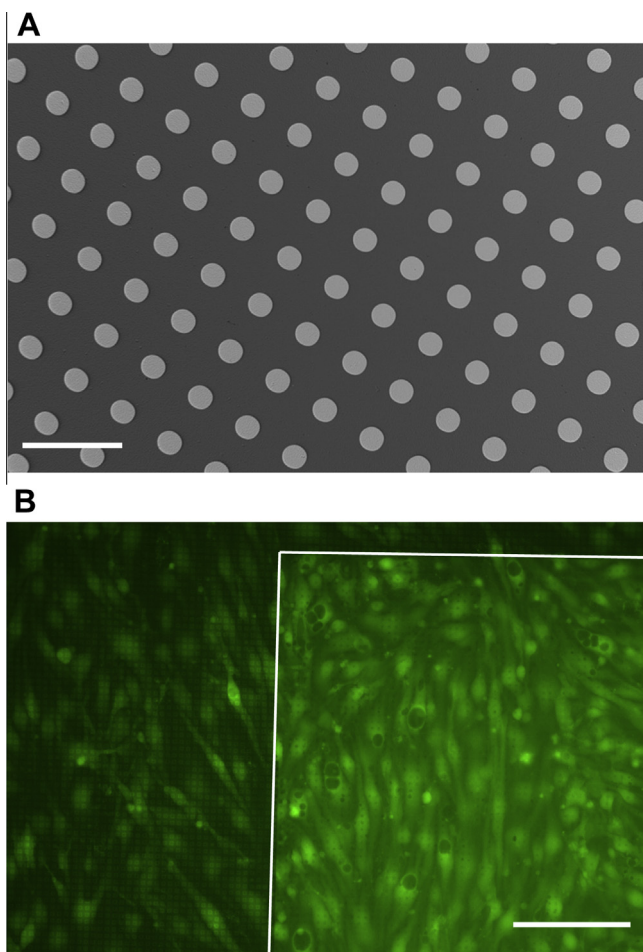


Fig. 5. Vacuole formation is not specific to pnc-Si. (A) TEM micrograph shows $3 \mu\text{m}$ diameter pores and $6 \mu\text{m}$ pore to pore spacing of silicon nitride (not pnc-Si) microporous membranes. Scale bar = $10 \mu\text{m}$. (B) Calcein AM-stained bEnd.3 cells expressed vacuoles only on free-standing microporous silicon nitride. Scale bar = $100 \mu\text{m}$.

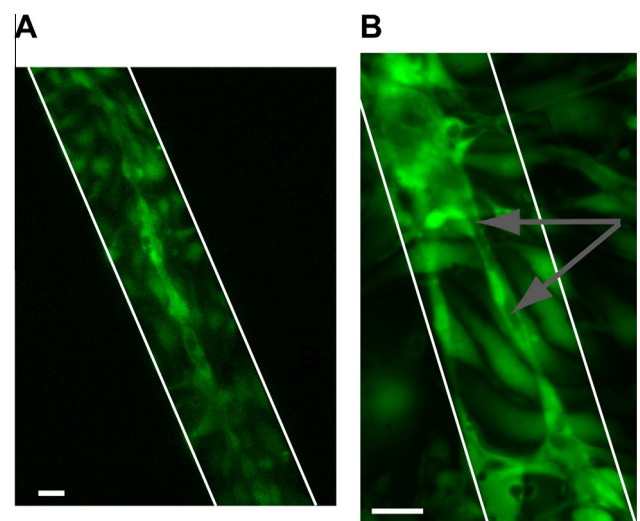


Fig. 6. Endothelial cells form tubes on pnc-Si transwells. (A) The bEnd.3 cells organized into 2-D tubes with closely apposed vacuoles, and were aligned with free-standing pnc-Si membrane areas. (B) Higher magnification of bEnd.3 on a pnc-Si transwell shows elongated endothelial cells with adjacent vacuoles (arrows) and branched structures. Scale bars = $30 \mu\text{m}$.

be a trigger for blood vessel formation. With fibroblasts, high basal permeability appears to trigger cell proliferation, which is also seen in healing tissue.

4. Discussion

While our previous study established pnc-Si as a viable cell culture substrate with cell adhesion and growth properties similar to glass [10], cells were not grown in a transwell format. Therefore, the impact of the high permeability of pnc-Si membranes [6] on cell behavior was not revealed. Here pnc-Si chips were suspended in custom-made transwell housings. Endothelial cells displayed vacuoles on regions of the chip where the membrane was free-standing but not in flanking regions where the pores of the membrane were blocked by the underlying silicon. Vacuoles were also seen when endothelial cells were cultured on permeable polymer and SiN substrates, but the degree of vacuole formation varied directly with substrate permeability. Both HUVECs and bEnd.3 endothelial cells responded to the free-standing membrane by displaying vacuoles but fibroblasts did not. After a few days, the endothelial cell culture appeared to undergo tubulogenesis with nascent vessels emanating from the free-standing membrane regions. Interestingly, fibroblasts appeared to proliferate and grow vertically over the free-standing membrane. These results suggest that basal permeability is an underappreciated microenvironmental parameter important for eliciting more tissue-like phenotypes in cell cultures.

Inspired by extensive literature documenting the impact of substrate compliance on cell phenotype [32,36,37], we considered an alternative hypothesis that cells were responding to the “softness” of the freely suspended pnc-Si membrane. We ruled this out by attaching a coverslip to the back of the pnc-Si chip, which limited the basal volume to ~ 300 nl (Supplementary Fig. 2). This approach effectively “chokes” off the basal permeability without changing membrane mechanics. Because no vacuoles were seen in cells on these modified transwells, the results point again to substrate permeability, not mechanics, as the environmental variable that leads to vacuole formation.

We also considered evidence that the hydraulic permeability of pnc-Si created conditions of continuous transcellular flow [38] and resulted in vacuole formation. In vivo, transcellular flow across cell monolayers can result from interstitial flow, which induces vacuole formation and capillary-like structures in human endothelial cells [17,19,39]. In our experiments, an imbalance in the media heights between apical and basolateral chambers of the transwells (e.g. hydrostatic pressure) inadvertently could result in transcellular flow. However, several experiments showed that transcellular flow is not the trigger of vacuoles in our experiments. First, b.End3 cells expressed vacuoles on low-porosity membranes with <2 nm pores (Fig. 4). Given the transwell dimensions, the maximum transcellular flow across these low-porosity pnc-Si membranes was $\sim 0.2 \mu\text{m s}^{-1}$. Much higher interstitial flow rates ($10 \mu\text{m s}^{-1}$) were used to induce vacuole formation in vitro [17,19,39], and hence the $0.2 \mu\text{m s}^{-1}$ flowrate of pnc-Si was an unlikely cause of vacuole formation. Furthermore, b.End3 cells expressed vacuoles on pnc-Si membranes with hydrostatic fluid flow blocked by a coverslip (Supplementary Fig. 2). Second, b.End3 cells expressed vacuoles on microporous SiN membranes (Fig. 5) even though the high hydraulic permeability of SiN membranes prevented an imbalance in media heights. Finally, while a basal to apical flow direction is necessary to induce vacuoles [38], vacuoles appeared regardless of the orientation of cells in the transwell (data not shown). Therefore, the high diffusive permeability of the membranes, not transcellular flow due to hydraulic permeability, appears to be the determinant of vacuoles in our studies.

The mechanisms by which permeability at the basal surface of cultured endothelial cells could trigger vacuole and tube formation are not yet clear. It is possible that when endothelial cells are grown on impermeable substrates such as TCPS or supported pnc-Si, biomolecules could be concentrated at basal cell surfaces and inhibit vacuole formation. By contrast, on permeable substrates such as free-standing pnc-Si or 3-D gels of ECM, these inhibitory factors could diffuse from the basal surfaces, thus enabling vacuole formation. For example, thrombospondin-1 (TSP-1) acts as an antiangiogenic signaling factor by binding to endothelial integrin receptors (i.e. CD36) and inhibiting many hallmarks of vasculogenesis [35,40]. TSP-1 is a large molecule (> 100 kD) however, and cells expressed vacuoles on low-porosity membranes with maximum pore sizes of <2 nm (<10 kDa). This result (Fig. 5) points to small protein fragments or peptide inhibitors of angiogenesis that are smaller than ~ 2 nm, rather than large protein inhibitors such as TSP-1. Peptide sequences with antiangiogenic activity have been identified on a multitude of larger proteins [41,42], and these can be smaller than the ~ 2 nm cut-off identified in our studies. For example, a ~ 150 amino acid domain of human histidine-rich glycoprotein (HRGP) has antiangiogenic activity in vivo, and can be cleaved endogenously from the larger HRGP protein via proteolytic activity [41]. The diffusion of antiangiogenic peptides or protein fragments from basal cell surfaces, enabled by substrate permeability, may be a key factor in driving vacuole and lumen formation in many angiogenesis assays.

5. Conclusions

This work showed an intriguing and physiologically relevant response in cultured endothelial cells that was specific to pnc-Si transwells. Unlike cells grown on less permeable substrates such as TCPS or polymer membranes, endothelial cells on pnc-Si transwells expressed vacuoles and formed multicellular networks that resembled capillary-like structures. These cells responded to the permeability of free-standing, nanoporous and nanothin pnc-Si membranes but not the membrane compliance or transmembrane fluid flow. Permeability at basal surfaces of endothelial cells may have allowed the dilution of an angiogenesis inhibitor, which we predict to be <2 nm. Pnc-Si transwells promoted vacuole and tube formation despite the lack of specialized stimuli (i.e. growth factors) in the cell culture media or 3-D ECM gels. Therefore, pnc-Si transwells are new, simpler devices with unique micro- and nanostructures that can be used to investigate how basolateral permeability alters cell behavior and morphology.

Disclosures

A corporate start-up, SiMPore Inc., participated in this work. SiMPore is working to commercialize the pnc-Si membrane material and two authors (T.G, J.M) affiliated with the original report of pnc-Si are founders of this start-up. N.N. was employed by SiMPore during this work. The company has partially funded this work through a New York State industry/academic partnership grant mechanism (CEIS).

Acknowledgements

The authors thank Dr. Alison C.P. Elder at the University of Rochester for helpful discussions and advice. We thank David Z. Fang for TEM and pnc-Si thermal treatments and Nikita Petukhov for assistance with diffusion experiments. We also thank Dr. Richard E. Waugh and Brian L. McIntyre who provided access to the AFM and SEM equipment in their laboratories at the University of Rochester. Financial support was provided by National Science

Foundation DMR0722653, the Center for Emerging and Innovative Sciences (CEIS), and SIMPore, Inc.

Appendix A. Figures with essential color discrimination

Certain figures in this article, particularly Figs. 1–6 are difficult to interpret in black and white. The full color images can be found in the on-line version, at <http://dx.doi.org/10.1016/j.actbio.2014.07.022>.

Appendix B. Supplementary data

Supplementary data associated with this article can be found, in the online version, at <http://dx.doi.org/10.1016/j.actbio.2014.07.022>.

References

- [1] Low SP, Williams KA, Canham LT, Voelcker NH. Evaluation of mammalian cell adhesion on surface-modified porous silicon. *Biomaterials* 2006;27:4538–46.
- [2] Low SP, Voelcker NH, Canham LT, Williams KA. The biocompatibility of porous silicon in tissues of the eye. *Biomaterials* 2009;30:2873–80.
- [3] Desai TA, West T, Cohen M, Boiarski T, Rampersaud A. Nanoporous microsystems for islet cell replacement. *Adv Drug Deliv Rev* 2004;56:1661–73.
- [4] Dalby MJ, Gadegaard N, Tare R, Andar A, Riehle MO, Herzyk P, et al. The control of human mesenchymal cell differentiation using nanoscale symmetry and disorder. *Nat Mater* 2007;6:997–1003.
- [5] Torchilin VP. Multifunctional nanocarriers. *Adv Drug Deliv Rev* 2006;58:1532–55.
- [6] Striemer CC, Gaborski TR, McGrath JL, Fauchet PM. Charge- and size-based separation of macromolecules using ultrathin silicon membranes. *Nature* 2007;445:749–53.
- [7] Gaborski TR, Snyder JL, Striemer CC, Fang DZ, Hoffman M, Fauchet PM, et al. High-performance separation of nanoparticles with ultrathin porous nanocrystalline silicon membranes. *ACS Nano* 2010;4:6973–81.
- [8] Snyder JL, Clark Jr A, Fang DZ, Gaborski TR, Striemer CC, Fauchet PM, et al. An experimental and theoretical analysis of molecular separations by diffusion through ultrathin nanoporous membranes. *J Membr Sci* 2011;369:119–29.
- [9] Kavalenka MN, Striemer CC, Fang DZ, Gaborski TR, McGrath JL, Fauchet PM. Ballistic and non-ballistic gas flow through ultrathin nanopores. *Nanotechnology* 2012;23:145706.
- [10] Agrawal AA, Nehilla BJ, Reisig KV, Gaborski TR, Fang DZ, Striemer CC, et al. Porous nanocrystalline silicon membranes as highly permeable and molecularly thin substrates for cell culture. *Biomaterials* 2010;31:5408–17.
- [11] Brightman MW, Reese TS. Junctions between intimately apposed cell membranes in the vertebrate brain. *J Cell Biol* 1969;40:648–77.
- [12] Gaillard PJ, Voorwinden LH, Nielsen JL, Ivanov A, Atsumi R, Engman H, et al. Establishment and functional characterization of an in vitro model of the blood-brain barrier, comprising a co-culture of brain capillary endothelial cells and astrocytes. *Eur J Pharm Sci* 2001;12:215–22.
- [13] Wuest DM, Wing AM, Lee KH. Membrane configuration optimization for a murine in vitro blood-brain barrier model. *J Neurosci Methods* 2013;212:211–21.
- [14] Bayless KJ, Davis GE. The Cdc42 and Rac1 GTPases are required for capillary lumen formation in three-dimensional extracellular matrices. *J Cell Sci* 2002;115:1123–36.
- [15] Davis GE, Black SM, Bayless KJ. Capillary morphogenesis during human endothelial cell invasion of three-dimensional collagen matrices. *In Vitro Cell Dev Biol: Anim* 2000;36:513–9.
- [16] Tolsma SS, Stack MS, Bouck N. Lumen formation and other angiogenic activities of cultured capillary endothelial cells are inhibited by thrombospondin-1. *Microvasc Res* 1997;54:13–26.
- [17] Vera RH, Genove E, Alvarez L, Borros S, Kamm R, Lauffenburger D, et al. Interstitial fluid flow intensity modulates endothelial sprouting in restricted src-activated cell clusters during capillary morphogenesis. *Tissue Eng Part A* 2009;15:175–85.
- [18] Ali S, Saik JE, Gould DJ, Dickinson ME, West JL. Immobilization of cell-adhesive laminin peptides in degradable PEGDA hydrogels influences endothelial cell tubulogenesis. *Biores Open Access* 2013;2:241–9.
- [19] Ng CP, Helm CL, Swartz MA. Interstitial flow differentially stimulates blood and lymphatic endothelial cell morphogenesis in vitro. *Microvasc Res* 2004;68:258–64.
- [20] Harris SG, Shuler ML. Growth of endothelial cells on microfabricated silicon nitride membranes for an in vitro model of the blood-brain barrier. *Biotechnol Bioprocess Eng* 2003;8:246–51.
- [21] Kuiper S, van Rijn CJM, Nijdam W, Elwenspoek MC. Development and applications of very high flux microfiltration membranes. *J Membr Sci* 1998;150:1–8.
- [22] Montesano R, Pepper MS, Mohle-Steinlein U, Risau W, Wagner EF, Orci L. Increased proteolytic activity is responsible for the aberrant morphogenetic behavior of endothelial cells expressing the middle T oncogene. *Cell* 1990;62:435–45.
- [23] Kamei M, Saunders WB, Bayless KJ, Dye L, Davis GE, Weinstein BM. Endothelial tubes assemble from intracellular vacuoles in vivo. *Nature* 2006;442:453–6.
- [24] Davis GE, Camarillo CW. An $\alpha 2\beta 1$ integrin-dependent pinocytic mechanism involving intracellular vacuole formation and coalescence regulates capillary lumen and tube formation in three-dimensional collagen matrix. *Exp Cell Res* 1996;224:39–51.
- [25] Bielaszewska M, Bauwens A, Greune L, Kemper B, Dobrindt U, Geelen JM, et al. Vacuolisation of human microvascular endothelial cells by enterohaemorrhagic *Escherichia coli*. *Thromb Haemost* 2009;102:1080–92.
- [26] Morissette G, Moreau E, C-Gaudreault R, Marceau F. Massive cell vacuolization induced by organic amines such as procainamide. *J Pharmacol Exp Ther* 2004;310:395–406.
- [27] Fang DZ, Striemer CC, Gaborski TR, McGrath JL, Fauchet PM. Methods for controlling the pore properties of ultra-thin nanocrystalline silicon membranes. *J Phys Condens Matter* 2010;22:454134.
- [28] Csoka B, Nagy G. Determination of diffusion coefficient in gel and in aqueous solutions using scanning electrochemical microscopy. *J Biochem Biophys Methods* 2004;61:57–67.
- [29] Fu BM, Curry FE, Weinbaum S. A diffusion wake model for tracer ultrastructure-permeability studies in microvessels. *Am J Physiol* 1995;269:H2124–40.
- [30] Sarkar R, Shaw AK, Narayanan SS, Dias F, Monkman A, Pal SK. Direct observation of protein folding in nanoenvironments using a molecular ruler. *Biophys Chem* 2006;123:40–8.
- [31] Kim E, Xiong H, Striemer CC, Fang DZ, Fauchet PM, McGrath JL, et al. A structure-permeability relationship of ultrathin nanoporous silicon membrane: a comparison with the nuclear envelope. *J Am Chem Soc* 2008;130:4230–1.
- [32] Guo WH, Frey MT, Burnham NA, Wang YL. Substrate rigidity regulates the formation and maintenance of tissues. *Biophys J* 2006;90:2213–20.
- [33] Wang Y, Kaiser MS, Larson JD, Nasevicius A, Clark KJ, Wadman SA, et al. Moesin1 and Ve-cadherin are required in endothelial cells during in vivo tubulogenesis. *Development* 2010;137:3119–28.
- [34] Gamble JR, Matthias LJ, Meyer G, Kaur P, Russ G, Faull R, et al. Regulation of in vitro capillary tube formation by anti-integrin antibodies. *J Cell Biol* 1993;121:931–43.
- [35] Koh JT, Kook H, Kee HJ, Seo YW, Jeong BC, Lee JH, et al. Extracellular fragment of brain-specific angiogenesis inhibitor 1 suppresses endothelial cell proliferation by blocking $\alpha v\beta 5$ integrin. *Exp Cell Res* 2004;294:172–84.
- [36] Hanjaya-Putra D, Yee J, Ceci D, Truitt R, Yee D, Gerecht S. Vascular endothelial growth factor and substrate mechanics regulate in vitro tubulogenesis of endothelial progenitor cells. *J Cell Mol Med* 2010;14:2436–47.
- [37] Higuchi A, Ling QD, Chang Y, Hsu ST, Umezawa A. Physical cues of biomaterials guide stem cell differentiation fate. *Chem Rev* 2013;113:3297–328.
- [38] Pedrigo RM, Simon D, Reed A, Stamer WD, Overby DR. A model of giant vacuole dynamics in human Schlemm's canal endothelial cells. *Exp Eye Res* 2011;92:57–66.
- [39] Swartz MA, Fleury ME. Interstitial flow and its effects in soft tissues. *Annu Rev Biomed Eng* 2007;9:229–56.
- [40] Dawson DW, Pearce SF, Zhong R, Silverstein RL, Frazier WA, Bouck NP. CD36 mediates the in vitro inhibitory effects of thrombospondin-1 on endothelial cells. *J Cell Biol* 1997;138:707–17.
- [41] Rosca EV, Koskimaki JE, Rivera CG, Pandey NB, Tamiz AP, Popel AS. Anti-angiogenic peptides for cancer therapeutics. *Curr Pharm Biotechnol* 2011;12:1101–16.
- [42] Olsson AK, Larsson H, Dixelius J, Johansson I, Lee C, Oellig C, et al. A fragment of histidine-rich glycoprotein is a potent inhibitor of tumor vascularization. *Cancer Res* 2004;64:599–605.